Supporting Information for

Hydrogen Migration, Surface Accumulation, and Nonradiative Recombination in Perovskite Solar Cells

Yong Huang[1, #], Xiqi Yang[1, #], Xiaoqing Chen[1, *], Rongkun Zhou[1], He Huang[1], Di Lu[1], Yongcai He[1], Wencai Zhou[2, *], Hui Yan[1], and Zilong Zheng[1, *].

[1] State Key Laboratory of Materials Low-Carbon Recycling, Beijing Key Lab of Microstructure and Properties of Advanced Materials, College of Materials Science and Engineering, School of Information Science and Technology Key Laboratory Optoelectronics Technology of Ministry of Education, Beijing University of Technology, Beijing 100124, China.

[2] Hubei Key Lab of Photoelectric Materials and Devices, School of Materials Science and Engineering, Hubei Normal University, Huangshi 435002, Hubei, China.

[#] Yong Huang, Xiqi Yang contributed equally to this paper.

* Correspondence Author (E-mail: zilong.zheng@bjut.edu.cn; chenxiaoqing@bjut.edu.cn; zwc@hbnu.edu.cn)

Computational Methods

All-atom molecular dynamics (AAMD) simulations:

All-atom molecular dynamics (AAMD) simulations were performed using the Large-scale Atomic/Molecular Massively Parallel Simulator (LAMMPS) package[1]. The equations of motion were integrated with a time step of 1 fs using the velocity-Verlet algorithm[2]. The perovskite surface was constructed from an 11 × 11 × 16 supercell of

$FAPbI_3$. Periodic boundary conditions applied for the x and y directions, along with a 150 Å vacuum on z direction. The atomic interactions within the perovskite were described by transferable perovskite force field[3]. Specifically, H_i was described using the OPLS-AA force field,[4] while its interactions with the perovskite lattice were parameterized based on the UFF force field.[5] The charge of H_i was set to +1e. The system was fully equilibrium at 300 K for 0.1 ns. Hydrogen interstitial (H_i) was inserted in the bulk region to simulate its migration from the interior toward the surface. The trajectories were propagated in NVT ensemble with Nosé-Hoover thermostat[6, 7] at 300 K for 1.2 ns to trace the diffusion trajectory and migration dynamics of H_i. The energy profile was obtained by: (i) selecting an equilibrated configuration at 300 K; (ii) choosing atomic positions along a linear path normal to the surface; (iii) introducing an H_i defect at each selected position; (iv) optimizing atomic positions and total energy via force minimization; and (v) collecting energy data as a function of position.

First-Principles Calculations:

All the first-principles calculations[8] were performed using the Vienna Ab initio Simulation Package (VASP)[9] with a plane wave basis set and projected augmented wave (PAW) [10] pseudopotentials. The equilibrium geometries were carried out using the Heyd-Scuseria-Ernzerhof (HSE)[11] hybrid functional in conjunction with spin-orbit coupling (SOC) effect. The Hartree-Fock exchange mixing parameter was set to 0.46, yielding a calculated band gap of 1.46 eV, agree with the experimental value of 1.47 eV[12]. All atoms were allowed to relaxed until the residual forces on each atom were less than 0.02 eV $Å^{-1}$. The plane-wave cutoff energy was set to 400 eV. Bulk defect calculations were performed using a 3 × 3 × 2 supercell sampled with a 2 × 2 × 2 Monkhorst-Pack k-point mesh. Surface calculations employed a 2 × 2 × 1 k-point mesh, with a vacuum region of 15 Å introduced along the z direction to eliminate spurious interactions between periodic images.

The defect formation energy of hydrogen interstitial was calculated using the formula[13]:

$$\Delta H^f\left(H_i^q\right) = E\left(H_i^q\right) - E(host) - \sum n_i(\mu_i + \Delta\mu_i) + q\left(E_F + E(VBM) + \Delta V\right) \quad \text{(S1)}$$

where $E\left(H_i^q\right)$ and $E(host)$ are total energies with and without defect, respectively. n_i indicates the number of defects added into the supercell. μ_i is the absolute value of the chemical potential of the defect atoms. $\Delta\mu_i$ stands for the relative value of the chemical potential, which is related to growth conditions. The Fermi energy E_F is referenced to the VBM of $FAPbI_3$, and $E(VBM)$ represents the energy of VBM. ΔV is a finite-size correction term for charged defects, which can be obtained with sxdefectalign package[14]. The transition level is defined as the Fermi-level position with respect to the bulk VBM, for which the formation energies of different defect charge states are equal:

$$\varepsilon\left(q/q'\right) = \left[E(a,q) - E\left(a,q'\right) - \left(q - q'\right)(E(VBM) + \Delta V)\right]/\left(q - q'\right) \quad \text{(S2)}$$

The carrier capture coefficient is determined using Fermi's golden rule

$$C = fV\frac{2\pi}{\hbar}gW_{if}^2\sum_m \Theta_m \sum_n \left|\langle\chi_{im}\left|\, Q - Q_0 \,\right|\chi_{fn}\rangle\right|^2 \delta\left(\Delta E + m\hbar\Omega_i - n\hbar\Omega_f\right) \quad \text{(S3)}$$

Where f is the Sommerfeld parameter accounting for the Coulombic interaction between the delocalized carrier (electron/hole) and charged defect. V, g, and Θ_m, represent the volume of the supercell, degeneracy factor of the final state, and the thermal occupation, respectively. Indices i and f label the initial and final electronic states, while m and n label the initial and final phonon states. W_{if} is the electron-phonon coupling matrix element, obtained with the NONRAD package[15]. χ_{im}/χ_{fn} are the ionic wave functions of initial/final states. Ω_i/Ω_f are the phonon frequencies of initial/final states. The δ function ensures the energy conservation during carrier capture[16]. After obtaining electron-phonon coupling, the capture coefficient are calculated with carriercapture.jl package[17], including the effect of lattice anharmonicity.

Nonadiabatic molecular dynamics (NAMD) simulations:

The nonradiative electron-hole recombination were investigated via nonadiabatic molecular simulations (NAMD) based on the semi-classical decoherence-induced surface hopping (DISH)[18, 19]. The DISH algorithm enables stochastic trajectory branching by introducing surface hopping events during electronic dephasing processes. The dephasing time, similar to the pure decoherence time in light-response theory, can be approximated by second-order cumulants[20]. This method has been widely applied to investigate the photo-excited charge dynamics in perovskites[21]. NAMD calculations were performed using the Hefei-NAMD program[22]. Based on the optimized geometries at 0 K, the temperature was equilibrium at 300 K for 3 ps with the NVT ensemble, then another 6 ps were produced in the NVE ensemble, and the last 3 ps trajectories were collected for the NA coupling and thermal fluctuations calculation[23]. We ran 1 ns NAMD simulations for each pair of states to calculate the rate constants for the electron-hole capture process.

Supporting Figures

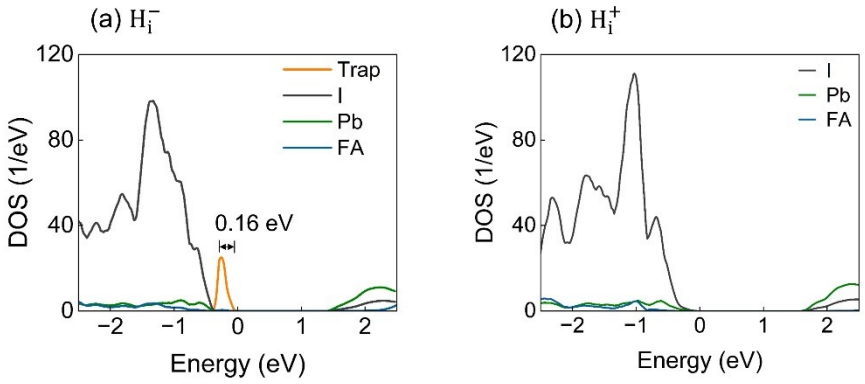

Figure S1. Projected densities of states (PDOS) of bulk hydrogen interstitial defects:

(a) H_i^- and (b) H_i^+.

Figure S2. PDOS of surface hydrogen interstitial defects: (a) H_i^- and (b) H_i^+.

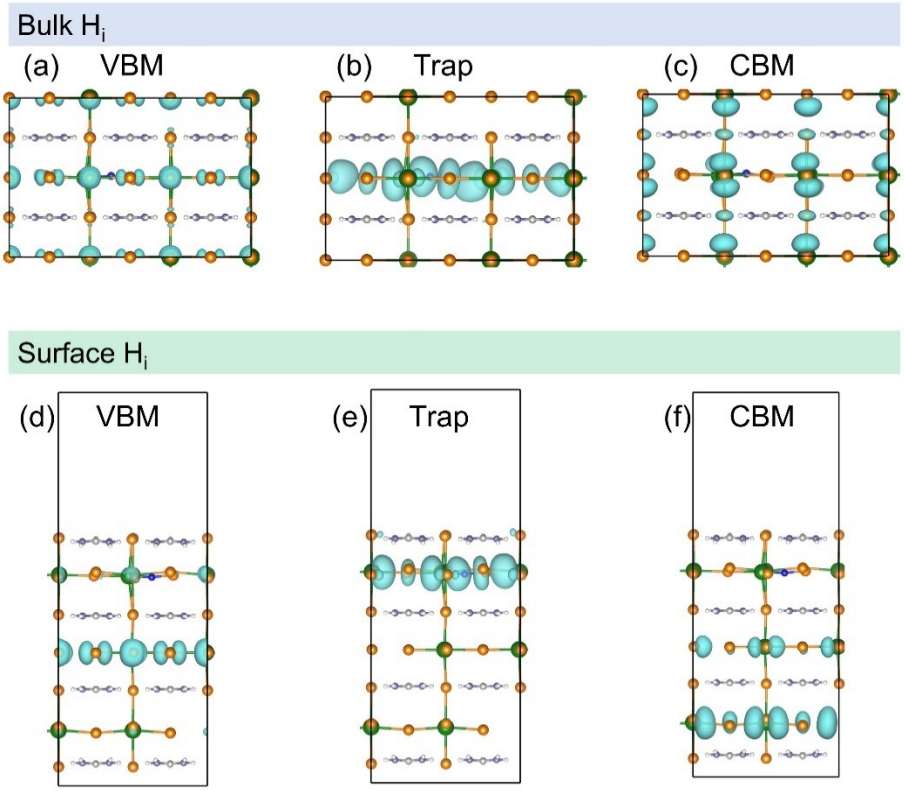

Figure S3. Charge density distributions of the key electronic states associated with H_i

in the bulk and at the surface of $FAPbI_3$. (a-c) Charge densities of the VBM, defect trap state, and CBM for bulk H_i. (d-f) Corresponding charge densities of the VBM, defect trap state, and CBM for surface H_i. All isosurfaces are plotted at the same value for direct comparison.

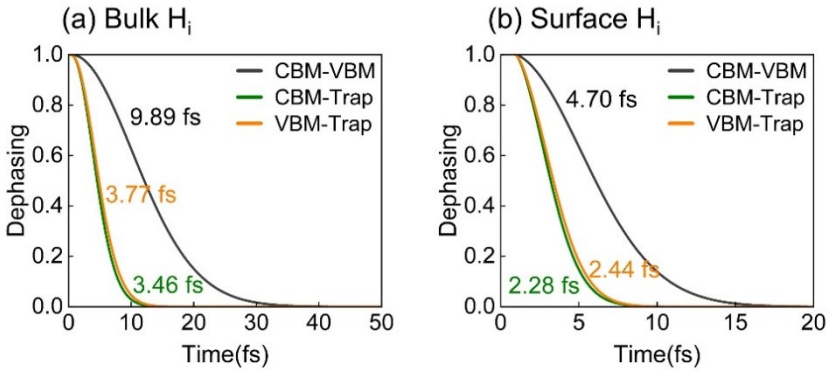

Figure S4. Dephasing functions for the key pairs of states in (a) bulk H_i and (b) surface H_i.

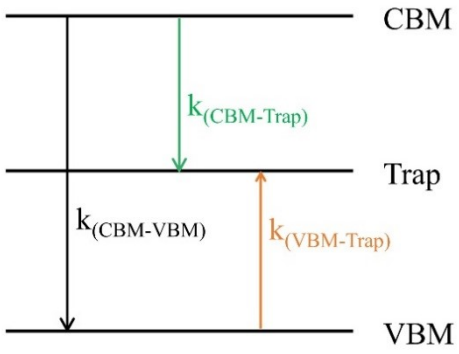

Figure S5. Schematic diagram of charge carrier recombination in H_i.

We focus on the dominant electron-trap-mediated charge recombination mechanism in the H_i defect system. Figure S5 schematically illustrates the carrier transition processes. The kinetic equations describing electron-hole recombination with electron trapping in the bulk H_i system is given in Equations S4-S6, whereas those describing electron-hole

recombination with hole trapping in the surface H_i system is provided in Equations S10-S12. Here, ES, Trap, and GS denote the populations of the excited, trap, and ground states, respectively, and $k_{(CBM\text{-}VBM)}$, $k_{(CBM\text{-}Trap)}$, and $k_{(VBM\text{-}Trap)}$ represent the transition rate constants for the CBM-VBM, CBM-Trap, and VBM-Trap processes, respectively (Figure S5). Figure S6 presents the nonadiabatic molecular dynamics (NAMD) data used to extract these transition rate constants.

Coupled kinetic equations describing electron-hole recombination with electron trapping at bulk H_i defects：

$$\frac{d[ES]}{dt} = -\left(k_{(CBM-VBM)} + k_{(CBM-Trap)}\right)[ES] \tag{S4}$$

$$\frac{d[Trap]}{dt} = k_{(CBM-Trap)}[ES] - k_{(VBM-Trap)})[Trap] \tag{S5}$$

$$\frac{d[GS]}{dt} = k_{(CBM-VBM)}[ES] + k_{(VBM-Trap)})[Trap] \tag{S6}$$

the solutions for this set of equations are:

$$[ES] = e^{-\left(k_{(CBM-VBM)} + k_{(CBM-Trap)}\right) * t} \tag{S7}$$

$$[Trap] = \frac{k_{(CBM-Trap)}}{\left(k_{(CBM-VBM)} + k_{(CBM-Trap)} - k_{(VBM-Trap)}\right)} e^{-k_{(VBM-Trap)} * t} - e^{-\left(k_{(CBM-VBM)} + k_{(CBM-T} \tag{S8}$$

$$[GS] = 1 - \frac{1}{\left(k_{(CBM-VBM)} + k_{(CBM-Trap)} - k_{(VBM-Trap)}\right)} \left\{ k_{(CBM-Trap)} * e^{-k_{(VBM-Trap)} * t} - \left(k_{(CBM} \right. \tag{S9}$$

Coupled kinetic equations describing electron-hole recombination with hole trapping at surface H_i defects：

$$\frac{d[ES]}{dt} = -\left(k_{(CBM-VBM)} + k_{(VBM-Trap)}\right)[ES] \quad \text{(S10)}$$

$$\frac{d[Trap]}{dt} = k_{(VBM-Trap)}[ES] - k_{(CBM-Trap)})[Trap] \quad \text{(S11)}$$

$$\frac{d[GS]}{dt} = k_{(CBM-VBM)}[ES] + k_{(CBM-Trap)})[Trap] \quad \text{(S12)}$$

the solutions for this set of equations are:

$$[ES] = e^{-\left(k_{(CBM-VBM)} + k_{(VBM-Trap)}\right)*t} \quad \text{(S13)}$$

$$[Trap] = \frac{k_{(VBM-Trap)}}{\left(k_{(CBM-VBM)} - k_{(CBM-Trap)} + k_{(VBM-Trap)}\right)} e^{-k_{(CBM-Trap)}*t} - e^{-\left(k_{(CBM-VBM)} + k_{(VBM-T} \quad \text{(S14)}$$

$$[GS] = 1 - \frac{1}{\left(k_{(CBM-VBM)} - k_{(CBM-Trap)} + k_{(VBM-Trap)}\right)} \left\{ k_{(VBM-Trap)} * e^{-k_{(CBM-Trap)}*t} - \left(k_{(CBM} \right. \quad \text{(S15)}$$

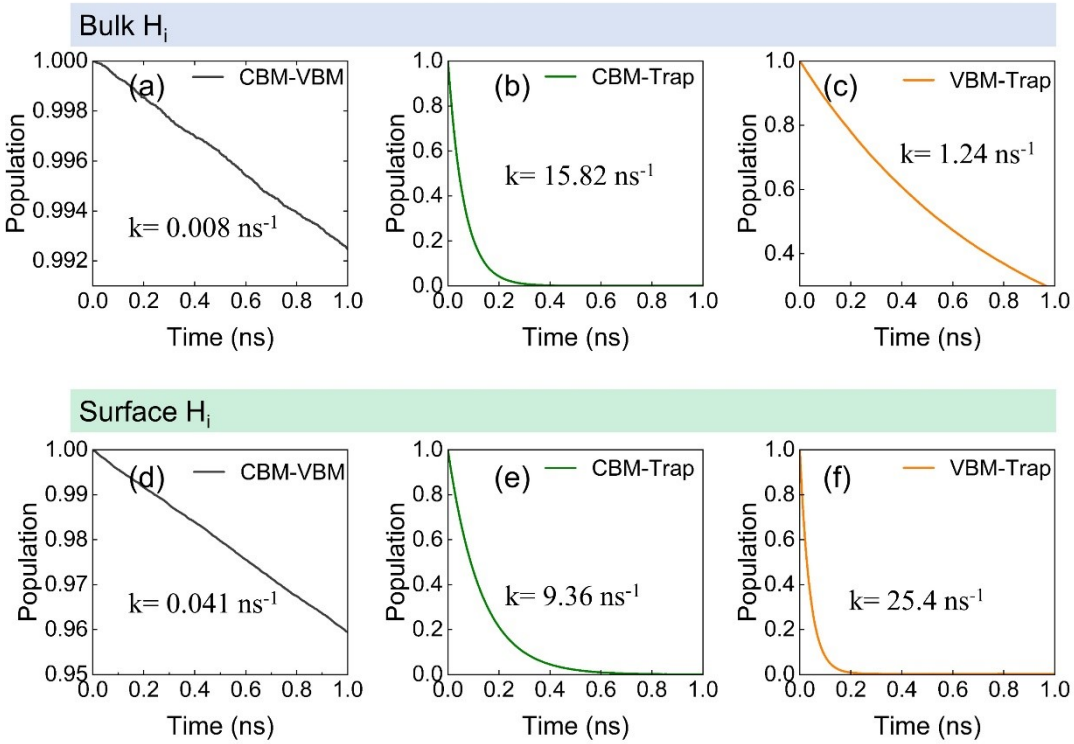

Figure S6. Time evolution of the populations of the key electronic states in the bulk and surface H_i systems. Shown are the population decays of the initially occupied states induced by carrier transitions for the bulk H_i system (a-c) and the surface H_i system (d-f). Specifically, panels (a, d) correspond to CBM-VBM transitions, (b, e) to CBM-Trap transitions, and (c, f) to VBM-Trap transitions.

Table S1. Non-adiabatic **(**NA) couplings, dephasing times, and trapping rates for bulk H_i and surface H_i.

		NA coupling(meV)	Dephasing (fs)	Rate (ns^{-1})
Bulk H_i	CBM-VBM	0.3	9.9	0.01
Surface H_i	CBM-VBM	0.2	4.7	0.04

References

1. A. P. Thompson, H. M. Aktulga, R. Berger, D. S. Bolintineanu, W. M. Brown, P. S. Crozier,

P. J. In't Veld, A. Kohlmeyer, S. G. Moore and T. D. Nguyen, Lammps-a flexible simulation tool for particle-based materials modeling at the atomic, meso, and continuum scales, Computer physics communications, 2022, 271, 108171.

2. L. Verlet, Computer" experiments" on classical fluids. I. Thermodynamical properties of lennard-jones molecules, Physical review, 1967, 159, 98.

3. J. A. Seijas-Bellido, B. Samanta, K. Valadez-Villalobos, J. J. Gallardo, J. Navas, S. R. G. Balestra, R. M. a. Madero Castro, J. M. Vicent-Luna, S. Tao and M. C. Toroker, Transferable classical force field for pure and mixed metal halide perovskites parameterized from first-principles, Journal of Chemical Information and Modeling, 2022, 62, 6423-6435.

4. G. A. Kaminski, R. A. Friesner, J. Tirado-Rives and W. L. Jorgensen, Evaluation and reparametrization of the opls-aa force field for proteins via comparison with accurate quantum chemical calculations on peptides, The Journal of Physical Chemistry B, 2001, 105, 6474-6487.

5. A. K. Rappé, C. J. Casewit, K. S. Colwell, W. A. Goddard Iii and W. M. Skiff, Uff, a full periodic table force field for molecular mechanics and molecular dynamics simulations, Journal of the American chemical society, 1992, 114, 10024-10035.

6. S. Nosé, A unified formulation of the constant temperature molecular dynamics methods, J. Chem. Phys., 1984, 81, 511-519.

7. W. G. Hoover, Canonical dynamics: Equilibrium phase-space distributions, Phys. Rev. A, 1985, 31, 1695-1697.

8. W. Kohn and L. J. Sham, Self-consistent equations including exchange and correlation effects, Physical review, 1965, 140, A1133.

9. G. Kresse and J. Furthmüller, Efficiency of ab-initio total energy calculations for metals and semiconductors using a plane-wave basis set, Computational materials science, 1996, 6, 15-50.

10. G. Kresse and D. Joubert, From ultrasoft pseudopotentials to the projector augmented-wave method, Physical review b, 1999, 59, 1758.

11. J. Heyd, G. E. Scuseria and M. Ernzerhof, Hybrid functionals based on a screened coulomb potential, The Journal of chemical physics, 2003, 118, 8207-8215.

12. M. T. Weller, O. J. Weber, J. M. Frost and A. Walsh, Cubic perovskite structure of black formamidinium lead iodide, α-$[hc(nh_2)_2]pbi_3$, at 298 k, The journal of physical chemistry letters, 2015, 6, 3209-3212.

13. J. Kang, J. Li and S.-H. Wei, Atomic-scale understanding on the physics and control of intrinsic point defects in lead halide perovskites, Applied Physics Reviews, 2021, 8.

14. C. Freysoldt, J. Neugebauer and C. G. Van de Walle, Fully ab initio finite-size corrections for charged-defect supercell calculations, Physical review letters, 2009, 102, 016402.

15. M. E. Turiansky, A. Alkauskas, M. Engel, G. Kresse, D. Wickramaratne, J.-X. Shen, C. E. Dreyer and C. G. Van de Walle, Nonrad: Computing nonradiative capture coefficients from first principles, Computer Physics Communications, 2021, 267, 108056.

16. A. Alkauskas, Q. Yan and C. G. Van de Walle, First-principles theory of nonradiative carrier capture via multiphonon emission, Physical Review B, 2014, 90, 075202.

17. S. Kim, S. N. Hood, P. van Gerwen, L. D. Whalley and A. Walsh, Carriercapture. Jl: Anharmonic carrier capture, Journal of Open Source Software, 2020, 5, 2102.

18. C. F. Craig, W. R. Duncan and O. V. Prezhdo, Trajectory surface hopping in the time-dependent kohn-sham approach<? Format?> for electron-nuclear dynamics, Physical review letters, 2005, 95, 163001.

19. E. R. Bittner and P. J. Rossky, Quantum decoherence in mixed quantum-classical systems: Nonadiabatic processes, The Journal of chemical physics, 1995, 103, 8130-8143.

20. S. Mukamel, Principles of nonlinear optical spectroscopy, (No Title), 1995.

21. W. Chu, Q. Zheng, O. V. Prezhdo, J. Zhao and W. A. Saidi, Low-frequency lattice phonons in halide perovskites explain high defect tolerance toward electron-hole recombination, Science advances, 2020, 6, eaaw7453.

22. Q. Zheng, W. Chu, C. Zhao, L. Zhang, H. Guo, Y. Wang, X. Jiang and J. Zhao, Ab initio nonadiabatic molecular dynamics investigations on the excited carriers in condensed matter systems, Wiley Interdisciplinary Reviews: Computational Molecular Science, 2019, 9, e1411.

23. G. Kresse and J. Furthmüller, Efficient iterative schemes for ab initio total-energy calculations using a plane-wave basis set, Physical review B, 1996, 54, 11169.